69

Comparison of Seismic Migration and Stripmap SAR Imaging methods for GPR for Landmine Detection

C. Gilmore, H.Su, I. Jeffrey, M. Phelan, and J. LoVetri
Department of Electrical and Computer Engineering, University of Manitoba, Winnipeg, Canada

Abstract: Various image reconstruction techniques used to image subsurface targets are reviewed. It is shown how some approximate wavefield inversion techniques: Stripmap SAR, Kirchhoff Migration (KM), and Frequency-Wavenumber Migration (F-K) are each developed by assuming different mathematical approximations and physical models for the wavefield scattering. The mathematical and physical model similarities are first delineated and it is shown that SAR is, computationally, almost identical to F-K migration. A plane wave interpretation of both SAR and F-K is used to show why they are so similar. Image reconstruction results for some of the methods, based on synthetic and experimental GPR data (SFCW), are then provided. Subjectively, the reconstructed images show very little difference, but computationally SAR (and, therefore, F-K migration) are much more efficient.

69.1 Introduction

The landmine detection problem is well known and electromagnetic (EM) techniques are only one method of solving it. One such standard EM technique is to construct an image of the subsurface wherein the landmine lies. Unfortunately, the general inverse EM problem is intractable, and therefore it is often usual to start with approximate physical models which do provide for efficient inverse solutions. Such models, which have come from seismic imaging studies in geophysics as well as from the synthetic aperture radar (SAR) arena, are the topic of this paper. In geophysics, these tomographic methods are usually referred to as migration techniques. Although the various techniques originate from a wide variety of physical models, the final imaging equations are surprisingly similar.

Conventional SAR imaging techniques are based on the convolution of the received data with the inverse of the point target response. This can be shown to be equivalent to the hyperbolic summation algorithm of geophysics.[1] It has been shown[1,2] that the more advanced (wave equation based) seismic migration techniques, Kirchhoff and Stolt Migration, are superior to this conventional

(convolutional) SAR. This superiority of the wave-based algorithms over hyperbolic summation has long been understood by geophysicists.

However, there are more sophisticated SAR-type algorithms, e.g., stripmap SAR,[3] that improve on conventional SAR. One of the purposes of this paper is to make clear the relationships between all these algorithms and to highlight their advantages and disadvantages. It is not well-known, for example, that the KM and F–K algorithms, both of which use the exploding source model, are theoretically identical (but see Ref. 4). We also show how the imaging equation for stripmap SAR, starting from a completely different formulation, is very similar to F–K and images obtained using each technique are subjectively the same. The relationship of stripmap SAR to the seismic migration algorithms is not well documented, and this is explored in Section 4.2.

We begin by reviewing the derivations of the stripmap SAR, hyperbolic summation (HS), Kirchhoff migration (KM), and frequency–wavenumber Migration (F–K) algorithms. The latter three techniques were first developed by the geophysical community whereas SAR is traditionally associated with RADAR. The stripmap SAR and HS algorithms are presented in 2D. This is typical of landmine GPR applications. On the other hand, the seismic algorithms we present in 3D form, but all algorithms can be derived for 2D. Comparisons are then made and image reconstruction results using stripmap SAR, KM, and F–K, based on synthetic and experimental GPR are subsequently provided. The experimental data are collected along a 1D line on the ground surface using a Vivaldi patch antenna and a vector network analyzer from 0.8 to 5 GHz. Both dielectric and metallic targets are buried in a dry silica sand ground environment.

69.2 Stripmap SAR

The stripmap SAR derivation begins by considering n point targets located in a two dimensional space with the ith target having coordinates (y_i, z_i), and reflectivity, σ_i. The general setup is shown in Figure 69.1.

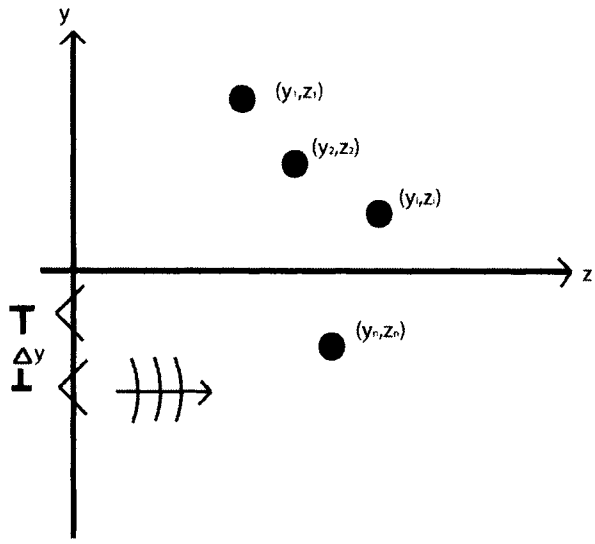

Figure 69.1 Stripmap SAR setup.

Assume that a radar emits a pulse $p(t)$ at each point on a set of equally spaced points on the y-axis, with a separation of Δy. The received signal $s(t, y)$ can then be modeled as:

$$s(t, y) = \sum_{i=1}^{n} \sigma_i p\left[t - \frac{2\sqrt{z_i^2 + (y_i - y)^2}}{c_m}\right] \tag{1}$$

where c_m is the velocity in the medium and as is usual in this derivation, we have neglected the attenuation term. If the Fourier Transform (FT), from the time domain, of the received signal $s(t, y)$ is taken, we get

$$S(\omega, y) = P(\omega) \sum_{i=1}^{n} \sigma_i e^{j2k\sqrt{z_i^2 + (y_i - y)^2}}, \tag{2}$$

where $k = \omega / c_m$ is the wavenumber, and $P(\omega)$ is the FT of the transmitted pulse.

If we then take the FT from the spatial domain and utilize the *method of stationary phase*,[3] we arrive at

$$S(\omega, k_y) = P(\omega) \sum_{i=1}^{n} \sigma_i e^{j\sqrt{4k^2 - k_y^2} z_i + j k_y y_i}, \tag{3}$$

where k_y is the spatial frequency. Here we have ignored a resultant amplitude term of $e^{-j\pi/4} / \sqrt{4k^2 - k_y^2}$ which results from the method of stationary phase.

We now note that if we define an ideal image for these point targets, as

$$g_o(y, z) = \sum_{i=1}^{n} \sigma_i \delta(y - y_n, z - z_n), \tag{4}$$

its FT would be

$$G_o(k_y, k_z) = \sum_{i=1}^{n} \sigma_n e^{j k_y y_i + j k_z z_i}. \tag{5}$$

Now, comparing Eqs. (3) and (5), identify

$$G_o(k_y, k_z) = \frac{S(\omega, k_y)}{P(\omega)}, \tag{6}$$

and make use of the so called spatial frequency mapping equation

$$k_z = \sqrt{4k^2 - k_y^2} = \sqrt{4\frac{\omega^2}{c_m^2} - k_y^2} \tag{7}$$

we can reconstruct the image by taking two dimensional inverse fourier transform (IFT) of the signal of Eq. (6). The final imaging equation is

$$F_{\mathrm{SAR}}(y, z) = \int\int \frac{S(\omega, k_y)}{P(\omega)} e^{j(k_y y + k_z z)} dk_y \, dk_z. \tag{8}$$

In order to evaluate Eq. (8), we require our data in the k_y, k_z domain. Unfortunately, if evenly spaced sample points are used in the ω domain, the use of Eq. (7) will result in nonuniformly spaced sample points in the k_z domain. Efficient evaluation of Eq. (8), using the fast fourier transform (FFT) algorithm requires evenly spaced points in both the k_z and the k_y domains. This requires

interpolation to find the value of $G_o(k_y, k_z)$ on a new, evenly spaced grid. This interpolation is the slowest part of the stripmap SAR algorithm.[3]

69.3 Seismic Migration Methods

Two types of Seismic migration will be considered here: Kirchhoff migration, and frequency–wavenumber (or Stolt) migration. Hyperbolic summation (or diffraction summation) will not be considered.

69.3.1 The Exploding Source Model

A fundamental principle of KM and F–K migration is the exploding source model. In the exploding source model it is assumed that the scattered field originates from sources located at the scatterers.[5] At time $t = 0$, these sources 'explode', and send traveling waves to the detectors at the surface. To adapt this new model, it is required that the velocity of propagation in the medium be taken as one half the original. Under this assumption wavefield migration consists of two concepts:

1. Backward extrapolation of the received signal to the exploding sources.
2. Defining the image as the backward extrapolated wavefield at time $t = 0$.

69.3.2 Kirchhoff Migration

Kirchhoff migration (KM) (or reverse-time wave equation migration, or wave field extrapolation) is based on an integral solution of the scalar wave equation: $\nabla^2\psi(\bar{r}, t) - \mu\varepsilon\partial_t^2\psi(\bar{r}, t) = 0$. This algorithm utilizes the exploding source model, so the velocity of propagation is $v = c_m/2$. The boundary conditions on the scalar wave equation specify ψ on the local ground surface (our collected data), and also specify that $\psi(\bar{r}, t) \to 0$ for $|\bar{r}| \to \infty$.

In order to simplify the final imaging integral equation the Green's function is chosen to satisfy the same wave equation, with Dirichlet conditions on the ground surface. Using the image principle, we get

$$G(\bar{r}, t|\bar{r}', t') = g(x, y, z, t|x', y', z', t') - g(x, y, z, t|x', y', -z', t') \tag{9}$$

where $g(\bar{r}, t|\bar{r}', t')$ is the free space Green's function:

$$g(\bar{r}, t|\bar{r}', t') = \frac{1}{4\pi}\frac{\delta(t - t' + R/v)}{R} \tag{10}$$

where $R = |\bar{r} - \bar{r}'|$. With this Green's function, the solution to the wave equation is given by the Kirchhoff integral as in Ref. 6:

$$\psi(\bar{r}, t) = -\int_{t'}\oint_{S'}\int \psi(\bar{r}', t')\frac{\partial G(\bar{r}, t|\bar{r}', t')}{\partial n'} - G(\bar{r}, t|\bar{r}', t')\frac{\partial}{\partial n'}\psi(\bar{r}', t')dS'dt' \tag{11}$$

where S' is the ground surface combined with the hemispheric half-space extending to infinity, and n' is the outward normal to the surface S'. Because $G(\bar{r}, t|\bar{r}', t') = 0$ and

$$\frac{\partial G(\bar{r}, t|\bar{r}', t')}{\partial n'} = 2\frac{\partial g(\bar{r}, t|\bar{r}', t')}{\partial n'}, \tag{12}$$

on S', we can write the scalar wave field as:

$$\psi(\bar{r},t) = -2\int \oint_{S'} \int \psi(\bar{r}',t')\frac{\partial g(\bar{r},t|\bar{r}',t')}{\partial z'}dS'dt', \tag{13}$$

where $n' = z'$ on the ground surface. This is known as the Rayleigh integral. Taking into account the following identity for the Green's function

$$\frac{\partial g(\bar{r},t|\bar{r}',t')}{\partial z'} = -\frac{\partial g(\bar{r},t|\bar{r}',t')}{\partial z}, \tag{14}$$

the scalar field can then be written as

$$\psi(\bar{r},t) = 2\frac{\partial}{\partial z}\int \oint_{S'} \int \psi(\bar{r}',t')g(\bar{r},t|\bar{r}',t')dS'dt'. \tag{15}$$

In the frequency domain, this scalar wave field solution can be written as in Ref. 4

$$\Psi(\bar{r},\omega) = 2\frac{\partial}{\partial z}\oint_{S'} \int \Psi(\bar{r}',\omega)g^*(\bar{r}|\bar{r}';\omega)dS', \tag{16}$$

where * denotes complex conjugate, and $g^*(\bar{r}|\bar{r}';\omega) = (1/4\pi)e^{-j\omega R/v}$.

Setting $t = 0$ in either Eq. (6), or the inverse FT of Eq. (16), leads to the final imaging equation for KM, but different practical implementations of KM will vary depending on the approximation used for the derivative, $\partial_z g(\bar{r},t|\bar{r}',t')$. For data obtained only on a line $(y', z' = 0)$, and when only the first two terms of the Taylor expansion for the derivative is used, the imaging equation becomes[7]

$$F_{\mathrm{KM}}(y,z) = \frac{1}{2\pi}\int \dot{\psi}(y',z'=0,R/v)\frac{\cos(\theta)}{vR} + \psi(y',z'=0,R/v)\frac{\cos(\theta)}{R^2}dy' \tag{17}$$

Where $\dot{\psi}$ is the time derivative of ψ, $R = \sqrt{(y-y')^2+z^2}$ and $\cos(\theta) = |z-z'|/R$. Note that two dimensional derivations of KM, utilizing the 2D Green's function are available.[7]

69.3.3 Frequency–Wavenumber Migration

Frequency–wavenumber (F–K), or Stolt migration was first developed by R.H. Stolt.[8] It is also based on a scalar wave equation model and the final result closely mirrors the final form of the stripmap SAR algorithm. Although the imaging equation is arrived at in a completely different manner, it has been shown to be theoretically identical to KM (see Section 3.4 and Ref. 4).

Again operating within the exploding source model, we consider a general plane wave:

$$\psi = e^{j\bar{k}\bullet\bar{R}-j\omega t} \tag{18}$$

where $\bar{R}$ is the position vector and the wavevector is $\bar{k} = k_x\hat{x} + k_y\hat{y} + k_z\hat{z}$. The magnitude of the wavevector is, $k = \omega/v$, and therefore by picking any three of the parameters k_x, k_y, k_z,ω the fourth becomes fixed.

A general field in time and space can be represented as a plane-wave expansion[8]:

$$\psi(x,y,z,t) = \int\int\int h(k_x,k_y,\omega)e^{j(k_x x+k_y y+k_z z)-j\omega t}dk_x\,dk_y\,d\omega \tag{19}$$

where $h(k_x, k_y, \omega)$ is an amplitude function of any three of the independent parameters. In GPR, we measure the field on the $z = 0$ plane: $\psi(x, y, 0, t) = p(x, y, t)$, and therefore we have

$$p(x, y, t) = \int\int\int h(k_x, k_y, \omega) e^{j(k_x x + k_y y) - j\omega t} dk_x\, dk_y\, d\omega. \tag{20}$$

Noting that this is a FT, we can determine the amplitude function as

$$h(k_x, k_y, \omega) = \left(\frac{1}{2\pi}\right)^3 \int\int\int p(x, y, t) e^{-j(k_x x + k_y y) + j\omega t} dx\, dy\, dt. \tag{21}$$

Utilizing the basic concepts of the exploding source model, the image we wish to display is

$$F_{\mathrm{FK}}(x, y, z) = \psi(x, y, z, 0) = \int\int\int h(k_x, k_y, \omega) e^{j(k_x x + k_y y + k_z z)} dk_x\, dk_y\, d\omega. \tag{22}$$

In order to utilize the efficiency of the Fast-Fourier transform algorithm, we make a change of variables from ω to k_z and the final imaging equation is

$$F_{\mathrm{FK}}(x, y, z) = \int\int\int \frac{v^2 k_z}{\omega} h(k_x, k_y, \omega) e^{j(k_x x + k_y y + k_z z)} dk_x\, dk_y\, dk_z. \tag{23}$$

This equation is the three dimensional inverse fourier transform (IFT) of the received data in the k_x, k_y and ω domain, multiplied by the Jacobian of the transformation from ω to k_z. In order to utilize the FFT, we again have the interpolation requirement that occurs in the SAR algorithm, but this time the interpolation equation is given by $k_z = \sqrt{k^2 - k_y^2}$. A very similar Eq. to (23) is obtained for F-K 2D imaging.

69.4 Discussion and Results

69.4.1 The Equivalence of Kirchhoff and Frequency–Wavenumber Migration

While the imaging Eqs.. (15) and (23), of KM and F–K migration look dissimilar, they are both solutions of the scalar wave equation back-propagated to time $t = 0$. It should come as no surprise that they are equivalent from a theoretical perspective. This can be shown as follows. A plane-wave expansion in the frequency domain can be expressed as:

$$\Psi(x, y, z, \omega) = \int\int h(k_x, k_y, \omega) e^{j(k_x x + k_y y + k_z z)} dk_x\, dk_y. \tag{24}$$

It can be shown (for $z < 0$) that [4]

$$\frac{\partial \tilde{g}^*(k_x, k_y, z; \omega)}{\partial z} = \frac{1}{2} e^{jk_z z}, \tag{25}$$

where $\tilde{g}(k_x, k_y, z; \omega)$ is the spatial FT of the free space Green's function for a source at the origin, $g(x, y, z; \omega) = (1/4\pi) e^{j\omega|\bar{r}/v|}$. By substituting into the plane-wave expansion in the frequency domain we arrive at

$$\Psi(x, y, z, \omega) = 2 \int\int h(k_x, k_y, \omega) \frac{\partial \tilde{g}^*(k_x, k_y, z; \omega)}{\partial z} e^{j(k_x x + k_y y)} dk_x\, dk_y. \tag{26}$$

Using that the FT of the product of two functions is the convolution of these functions we get the ω domain representation of KM Eq. (16).

69.4.2 Comparison of the Different Methods

While the two wave equation based solutions (KM and F–K) are theoretically the same, the practical use of the two algorithms is different. The two major differences are the approximation of the derivative of the Green's function, and the computational efficiency. Use of the FFT algorithm in F–K migration greatly reduces computational time (the interpolation step is the slowest step in the algorithm).

The final imaging equations for the SAR algorithm and for the F–K algorithm are very similar. The differences are the multiplication of the Jacobian of the transformation from $d\omega$ to dk_z and the division of the data by $P(\omega)$. Although it first seems that the interpolation equations are different, when we consider the modified exploding source model velocity used in F–K migration, the equations become the same.

Another way to see the similarities between stripmap SAR and F-K migration algorithms is by reconsidering the stripmap SAR derivation. If we assume an exploding source that emanates a plane wave from the source point (y_i, z_i), to the receiving point $(y, 0)$ the received data can be represented as

$$\begin{aligned} S(y,\omega) = P(\omega, y)e^{j\bar{k}\cdot\bar{R}} &= P(\omega, y)e^{j\frac{\omega}{v}\frac{(-z_n)(-z_n)+(y-y_n)(y-y_n)}{\sqrt{z_n^2+(y-y_n)^2}}} \\ &= P(\omega, y)e^{jk\sqrt{z_n^2+(y-y_n)^2}}, \end{aligned} \tag{27}$$

where $P(\omega, y)$ takes into account both the pulse shape and the reflectivity. We can easily see, with $v = c_m/2$, that this is equivalent to Eq. (2). Given that Eq. (2) is really a plane wave expansion of the received field, using the same techniques as were used in the sum of plane waves derivation of F–K migration, we could determine $P(\omega, k_y)$. As we did in F–K migration, we could then determine the field at time $t = 0$, which we have identified as the image. However, as was previously shown, it is usual in stripmap SAR to derive the final imaging equation by analogy to the inverse FT of a point source located at the scattering centres. No reference to the solution of the wave equation is ever made in stripmap SAR. This is the difference between stripmap SAR and the F–K algorithms.

In terms of actual imaging, we have found very little difference which would justify use of KM. Shown in Figure 69.2 are the unfocused, F–K and KM images for the synthetic data corresponding to two point targets. The data simulates that which would be collected by a 1 to 12.4 GHz SFCW radar. The only notable difference was computation time, with F–K migration taking over two orders of magnitude less time than KM. The root-mean-square (RMS) error between these images and an ideal point image was calculated to be approximately the same. Although not shown, the stripmap SAR image for the same synthetic data was created, and as expected, very little difference was observed.

Experimental data was also obtained, using a monostatic setup with a Vivaldi patch antenna and a VNA from 0.8 to 5 GHz, for three dielectric and one metal target buried in dry silica sand. The results of the three focusing algorithms are

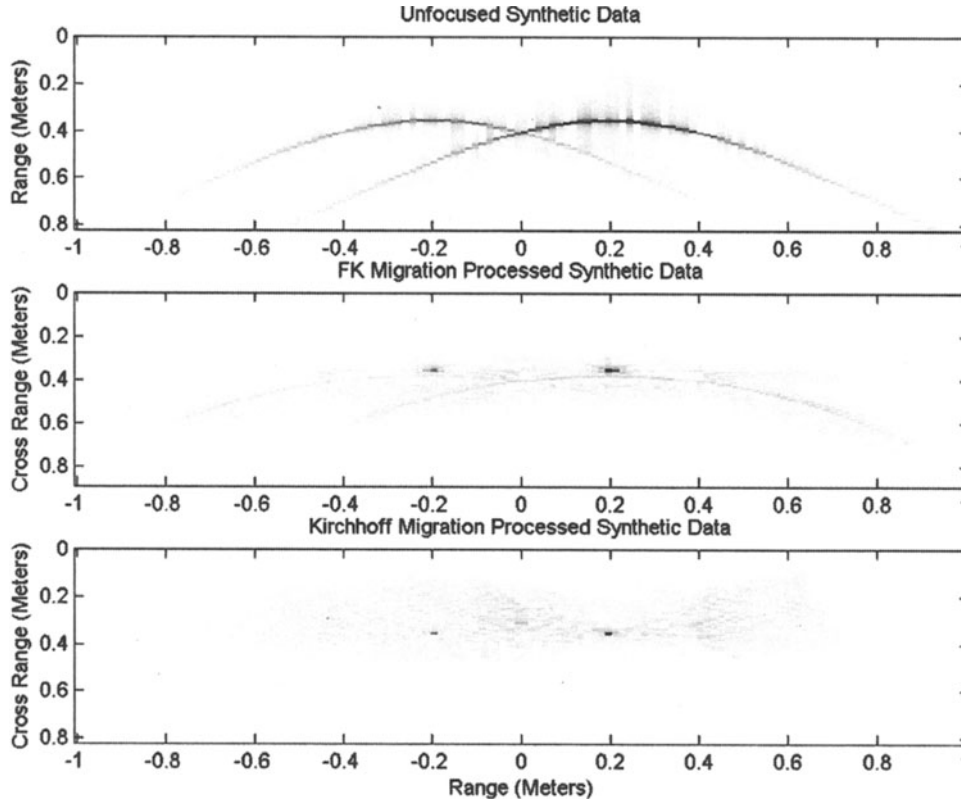

Figure 69.2 F-K and KM of synthetic data 2 targets, synthetic 1 to 12.4 GHz SFCW data.

shown in Figure 69.3. Here, the ground surface has been windowed out of the image to enhance the targets. From left to right, the targets are two rectangular mine shaped dielectric targets, a small piece of wood, and a small piece of metal. While the KM result looks slightly different than the other two images, the only major difference between the three algorithms was computation time. The KM algorithm again took two orders of magnitude longer than the stripmap SAR and F–K algorithms.

69.5 Conclusion

We have shown how various migration algorithms, which can be applied to GPR imaging of landmines, are developed, and shown the similarities and differences both from a theoretical and computational point of view. Images formed by these algorithms show little subjective difference. The main difference is computational time and it was shown that stripmap SAR and F–K migration are much more computationally efficient than KM. Confusion around the close relationship between stripmap SAR and F–K algorithms was alleviated by using a sum of plane waves interpretation of both techniques.

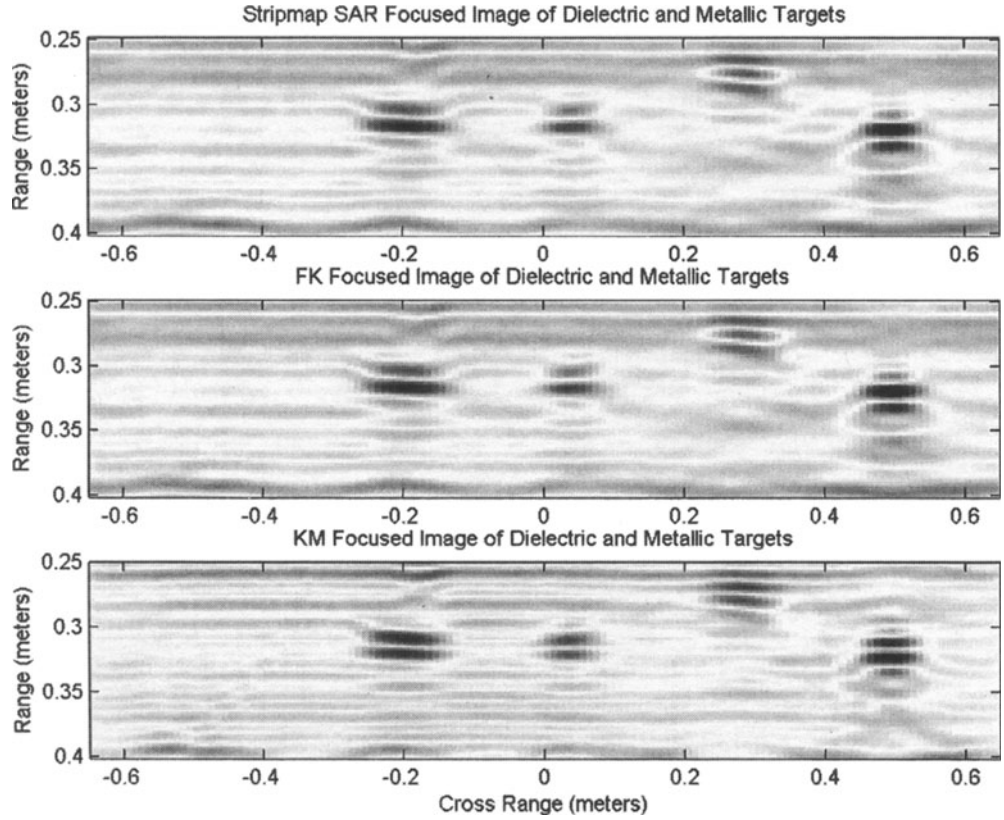

Figure 69.3 Stripmap SAR, F-K, and KM images of experimental 0.8 to 5 GHz SFCW radar.

References

1. A. Gunawardenda and D. Longstaff, Wave equation formulation of synthetic aperture radar (SAR) algorithms in the time-space domain, *IEEE Trans. Geosci. Remote Sens.*, **36**(6) (1998).
2. C. Cafforio, C. Prati, and F. Rocca, SAR data focusing using seismic migration techniques, *IEEE Trans. Geosci. Remote Sens.*, **27**, 194–207 (1991).
3. M. Soumekh, *Synthetic Aperture Radar*, Chapter 4, John Wiley & Sons, New York, 1999.
4. M. S. Zhdanov, *Geophysical Inverse Theory and Regularization Problems*, Elsevier, Amsterdam, 2002.
5. J. F. Claerbout, *Imaging the Earths Interior*, Blackwell Scientific Publications, Oxford, 1985.
6. Morse and Feshbach, *Methods of Theoretical Physics*, vol. 1, Section 7.3, McGraw-Hill, NY, USA, 1953.
7. W. A. Schneider, Integral formulation for migration in two and three dimensions, *Geophysics*, **43**, pp. 49–76 (1978).
8. R. H. Stolt, Migration by Fourier transform, *Geophysics*, **43**(1), pp. 23–48 (1978).
9. J. S. Stratton, *Electromagnetic Theory*, McGraw-Hill, NY, 1941, p. 363.